Research Article

# Removal of Propylparaben in an Aqueous System using Magnetite-Silica Ferrofluids of Hydrophobic Deep Eutectic Solvent

Aswin Falahudin
Department of Chemistry, Faculty of Science, Chulalongkorn University, Bangkok, Thailand

Numpon Insin*
Department of Chemistry, Faculty of Science, Chulalongkorn University, Bangkok, Thailand
Photocatalysts for Clean Environment and Energy Research Unit, Faculty of Science, Chulalongkorn University, Bangkok, Thailand

* Corresponding author. E-mail: Numpon.i@chula.ac.th DOI: 10.14416/j.asep.2024.03.001
Received: 15 November 2023; Revised: 20 December 2023; Accepted: 17 January 2024; Published online: 18 March 2024


**Abstract**
A novel sorbent based on ferrofluid hydrophobic deep eutectic solvent magnetite silica ($Fe_3O_4$@$SiO_2$@m$SiO_2$-HDES) was successfully synthesized by adding menthol-fatty acid as carrier liquid onto $Fe_3O_4$@$SiO_2$@m$SiO_2$ composite. The crystallinity, morphological, functional group and magnetic properties of the materials were characterized by x-ray diffraction, scanning electron microscopy-EDX, Brunauer–Emmett–Teller, vibrating sample magnetometer, thermogravimetric analysis and Fourier Transform-infrared spectroscopy. The adsorption performance of parabens was evaluated as model water pollutants. The $Fe_3O_4$@$SiO_2$@m$SiO_2$-HDES ferrofluid was used as a ferrofluid sorbent of parabens prior to spectrophotometry UV-Vis. The effect of several contribution parameters was optimized including ferrofluid volume, pH, stirring time and ionic strength. Under the optimum conditions, a combination of $Fe_3O_4$@$SiO_2$@m$SiO_2$-menthol/palmitic acid was achieved as the best ferrofluid with % removal values ranging from 81.00% to 98.62%. The ferrofluid $Fe_3O_4$@$SiO_2$@m$SiO_2$-HDES demonstrated high efficiency for the adsorption paraben in the water system which suggests a great potential alternative method for the adsorption of water contaminants in the aquatic system.

**Keywords**: Ferrofluid, Hydrophobic deep eutectic solvent, Magnetic phase extraction, Parabens

## 1 Introduction

The rapid growth of industrial and urbanized areas has become a concern, especially regarding the impact on water pollutants. Pharmaceuticals, pesticides, and personal care products are widely produced and consumed ingredients that contribute to water pollution. Some substances in the product resist biodegradation and tend to accumulate, posing a significant hazard to aquatic life [1]. Parabens are derivatives of ester compounds formed from para-hydroxybenzoic acid and alkyl chains, commonly used as preservative compounds in various product industries due to the properties offered such as low cost, odorless, colorless, and chemical stability [2]. However, previous studies have shown that pollution and the continuous accumulation of parabens in low concentrations in our bodies over the long term can cause breast cancer [3]. Some reports about the propylparaben compound can cause abnormality in the endocrine system. The regulation of propylparaben has been arranged at 0.14% and 2 mg/day for cosmetics and food, respectively [4]. In addition, contamination of propylparaben in our bodies may occur via wastewater that is polluted from industry and domestic waste from our daily care products. The data confirmed that propylparaben has been detected in our aquatic system (ng/L to µg/L), such as in groundwater in Poland [5], the Turia River

in Valencia, Spain [6], wastewater in Germany [7], and the Pearl River Estuary in South China [8]. It has grown into a major global health issue. Currently, technologies have been developed to minimize wastewater from water systems have been developed, such as enzymatic reaction [9], radiation [10], solvent extraction [11], ion exchange [12], precipitation [13], and electrochemical [14]. However, other reports indicate that applying these technologies creates toxic byproduct, decomposes nutrient, and requires expensive equipment [15]. The biggest challenge to minimizing labor equipment and safety to environmental, sorbent technology was offering high-efficiency removal and eco-friendliness.

Zeolite [16], activated carbon [1], and Metal-Organic Frameworks [17] are common adsorbents to remove water contaminants. In recent years, ferrofluid technology-based magnetic materials have received great attention as adsorbent technology due to their effectiveness as adsorbent. Ferrofluid is a stable magnetic colloid and homogeneous dispersion of magnetic material in a carrier solvent. As a sorbent material, ferrofluid offers quick and easy operation [18].

Iron oxide is the most popular magnetic material widely used as a magnetic core due to its stability and magnetic response. Magnetite ($Fe_3O_4$) is among the best candidates for ferrofluids due to its superparamagnetic properties, biocompatibility, and low toxicity, which can improve the adsorbent with eco-friendly properties [19]. However, instability, easy corrosion, and agglomeration were major problems with magnetite particles [20]. The strategy of coating magnetite material not only improves the stability but also enhances the surface area of particles. The silica layer is an inorganic material that becomes an outstanding candidate for coating due to its large porosity, biocompatibility, easy surface functionalization, and adjustable pore structure [21]. Mesoporous silica is a type of silica structure with a higher surface area that can improve the active site as an adsorbent. Moreover, a large number of porous silica can effectively adsorb analyte [22]. To the best of our knowledge, few reports use a combination of shell and mesoporous structure silica in ferrofluid technology for propylparaben adsorption.

On the other hand, the carrier liquid is also important to construct a highly effective ferrofluid. Recently, traditional carrier liquids such as organic solvent, water, and ethylene glycol were applied to ferrofluids. Even though magnetic materials can disperse in their liquids, these carrier liquids cannot act as extraction solvents [23]. The deep eutectic solvent (DES) is a new carrier liquid consisting of a hydrogen bond donor and hydrogen acceptor. Since it was discovered, deep eutectic solvents offer unique properties, such as high liquid purity, simple preparation, low-cost production, and liquid form at room temperature, so that DES form has a low melting point when compared to individual compounds [24]. In addition, deep eutectic solvents are also known as green solvents, so they are extensively used in many different reactions [25]. The issue of instability DES is the main problem when it is applied. Hydrophobic deep eutectic solvent (HDES) resolves the problem of instability DES in a water system. HDES has unique properties as a carrier liquid due to high stability and low water content after its use in water systems [26]. Hydrophobic Natural deep eutectic solvent (NADES) has recently developed from the hydrophobic deep eutectic solvent with natural compounds as basic materials and represents the green chemistry principle. Hydrophobic NADES have been utilized in separation science such as doxycycline (DOC) [27] and cinnamic acid [23].

In this work, synthesized ferrofluid composed of hydrophobic NADES-magnetite modified silica shell and mesoporous by a simple method. $Fe_3O_4$-modified silica and mesoporous silica were utilized as magnetic components. The high surface area of the silica facilitates the adsorption of propylparaben via a porous structure. Combination with menthol/fatty acid as a carrier liquid can enhance the effectiveness of removal of paraben wastewater in an aqueous system. The proposed hydrophobic NADES in ferrofluid increases the sorption effectiveness and facilitates the separation of sorbent and analytes by utilizing the differences in density and magnetic force [18].

## 2 Experimental

### 2.1 *Materials*

Iron(II) sulfate heptahydrate (99%), iron(III) chloride (97%), menthol (99%), decanoic acid (98%), palmitic acid (98%), stearic acid (95%), tetraethyl orthosilicate (98%), and cetyltrimethylammonium bromide

(98%) were purchased from Sigma-Aldrich. Methyl 4-hydroxybenzoate (99%), ethyl 4-hydroxybenzoate (99%), and butyl 4-hydroxybenzoate (99%) were obtained from Thermo Scientific. Lauric acid and propyl 4-hydroxybenzoate (99%) were obtained from the Tokyo chemical industry. Ammonia solution (25%) and sodium hydroxide (99%) were supplied from Merck.

### 2.2 *Ferrofluid preparation*

#### *2.2.1 Synthesis of coated with a silica shell and mesoporous silica ($Fe_3O_4$@$SiO_2$@$mSiO_2$)*

$FeSO_4.7H_2O$ (0.54 g) and $FeCl_3.6H_2O$ (0.31 g) were dissolved in 150 mL milli-Q water. After that, 1 M NaOH solution was added slowly until a pH reached 10–11, and the reaction mixture was stirred vigorously at 70 ºC for 2.5 h. The external magnet separated the formation of black suspension and many times washed with deionized water and ethanol [28]. The next step was to coat the $Fe_3O_4$ with a silica shell by combining 100 mg of $Fe_3O_4$ in ethanol: water solution (1:4) and sonicated for 5 min. Then tetraethyl orthosilicate (300 µL) and ammonia solution (400 µL) were added slowly into the system twice after 10 minutes of reaction. The mixture was stirred for 24 h at room temperature. In addition, the suspended particles $Fe_3O_4$@$SiO_2$ were washed with deionized water and ethanol, followed by drying in an oven overnight [29]. To create mesoporous on the surface, $Fe_3O_4$@$SiO_2$ (0.4 g) was dissolved into a 35:15:2 water-ethanol-NaOH solution (V/V), followed by 30 minutes of sonication. Then, cetyltrimethylammonium bromide (50 mL) was slowly added until a homogeneous colloidal suspension was formed. The mixture was heated at 80 °C for 4 h. After that, ethanol (5 mL) was added, followed by tetraethyl orthosilicate (1 mL), before stirring for 2 h to form a dark-brown colloid suspension and aging the mixture for 18 h at room temperature. The product was washed with deionized water and ethanol and dried overnight. The powder-dried colloid was calcined at 540 °C for 6 h, which aims to remove CTAB. The mesoporous structure was investigated by nitrogen adsorption-desorption isotherm analysis [30].

#### *2.2.2 Preparation of hydrophobic DES*

Menthol and fatty acid with different molar ratios were combined in bottles of glass and heated for 30 min at 80 °C until a clear liquid solution was formed to create hydrophobic DES. The solution hydrophobic DES was cooled to room temperature (Details are provided in the supporting information, Table S1) [31].

#### *2.2.3 Synthesis of ferrofluids*

50 mg of $Fe_3O_4$@$SiO_2$@$mSiO_2$ particles were dispersed in 1.5 mL of hydrophobic DES. Then, the mixture was vortex for 5 min, followed by sonication for 1 h to prevent the formation of particle clusters and to obtain stable ferrofluids. Other ferrofluids were also prepared by different liquid carrier mass and ratios of $Fe_3O_4$@$SiO_2$@$mSiO_2$: Hydrophobic DES (Table S2) [23].

### 2.3 *Sorption study*

The sorption of propylparaben onto ferrofluid was conducted by batch sorption method. About 5 mL of propylparaben 10 mg/L aqueous solution was prepared in the bottle samples, and 200 µL of ferrofluid was added to the solution. The mixture was stirred at 300 rpm at room temperature for 30 min. After that, an external magnet was applied to separate the sorbent from the solution. In the next step, the mixture solution was filtered through a 0.22 filter membrane before analysis using a UV-Vis spectrophotometer. The removal efficiency (% R) was calculated according to Equation (1),

$$Removal = \frac{(C_0 - C_e)}{C_0} \times 100\% \quad (1)$$

### 2.4 *Characterization*

Iron oxide and their composite were carried out using X-ray diffraction (Rigaku-Smartlab) to determine the crystal phases, and the functional groups of materials were obtained using FTIR (Thermo Nicolet iS50). The images and elemental composition were obtained using SEM-EDX (JEOL IT-100, Japan). The TGA was performed through the application Pyris manager (Pyris 1), and the surface area for all samples was measured by an adsorption analyzer (BELSORP-mini II). Magnetization measurements were performed with a vibrating sample magnetometer (VSM), and a

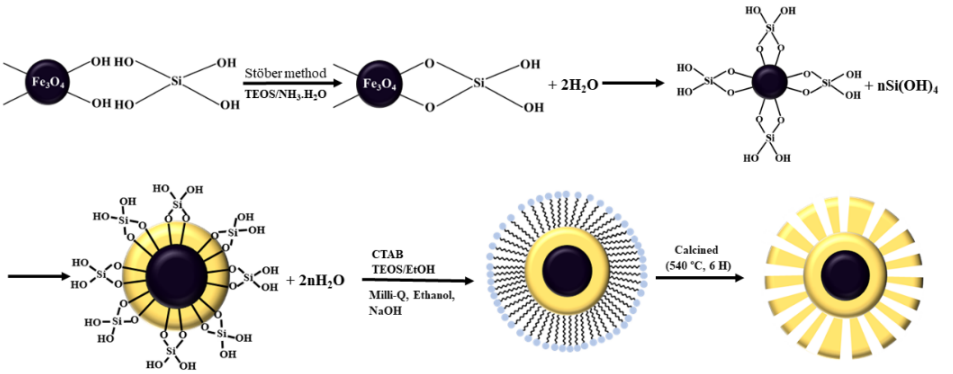


**Figure 1**: General schematic illustration of $Fe_3O_4$@$SiO_2$@m$SiO_2$ synthesis.

spectrophotometer UV-Vis was used to identify water pollutant concentration during the adsorption study (Agilent-8453).

## 3 Result and Discussion

### 3.1 *Synthesis of $Fe_3O_4$ coated silica shell and mesoporous silica*

$Fe_3O_4$ particles are synthesized using the co-precipitation method approach. Initially, $Fe^{2+}$ and $Fe^{3+}$ dissolved in the solution underwent hydrolysis with the addition of sodium hydroxide to the depth of the solution. Then, $Fe^{2+}$ and $Fe^{3+}$ ions were formed into $Fe(OH)_3$ and $Fe(OH)_2$, and slowly transformed to $Fe_3O_4$ precipitates as indicated by black precipitation, under the following reactions in Equations (2)–(4) [32].

$$Fe^{3+} + 3OH^- \rightarrow Fe(OH)_3 \quad (2)$$

$$Fe(OH)_3 \rightarrow FeOOH + H_2O \quad (3)$$

$$Fe^{3+} + 2OH^- \rightarrow Fe(OH)_2 \quad (4)$$

$$2FeOOH + Fe(OH)_2 \rightarrow Fe_3O_4\downarrow + 2H_2 \quad (5)$$

Surface protection of magnetite was achieved by coating silica shells and mesoporous silica (Figure 1). Stöber method was used to create the silica shells layer in ethanol-ammonia by hydrolysis and polycondensation of TEOS [33], yielding brown magnetic particles for the final product. Utilizing CTAB as a template in a basic solution, the sol-gel process was used to create the mesoporous structure of silica. The template was then removed through calcination, generating a porous structure [30].

### 3.2 *Characterization and identification of material*

The crystallinity and composition of the materials have been characterized using X-ray diffraction (XRD). The XRD pattern of bare magnetite and composites is presented in Figure 2. The characteristic diffraction peaks at 2θ = 30.06º, 35.42º, 43.16º, 53, 62º, 56, 97º, 62.56º in the XRD pattern, which is indicative of crystallization of the pure magnetite ($Fe_3O_4$) phase of iron oxide (JCPDS No. 19-0629) [33]. Successfully silica coating on magnetite can be observed with a broad peak at 2θ = 20–25° in the XRD pattern, for all composite $Fe_3O_4$@$SiO_2$, $Fe_3O_4$@m$SiO_2$, and $Fe_3O_4$@$SiO_2$@m$SiO_2$ that corresponding diffraction peak of $SiO_2$ [30]. The result suggested that $SiO_2$ existed on the surface of magnetite. The XRD patterns of all composites after silica coating showed that the intensity of the XRD peaks of pure $Fe_3O_4$ was decreased but still observed, which is associated with the reduced crystalline properties of $Fe_3O_4$ impact of the encapsulated with amorphous silica [29].

SEM-EDX determined the surface morphology and elemental analysis of bare magnetite and composites. Figure 3(a). SEM image of $Fe_3O_4$ confirmed that the particles look not uniform and have a rough surface. After $Fe_3O_4$ particles coated with a silica layer on the surface, the particles of $Fe_3O_4$@$SiO_2$ [Figure 3(b)] were showed uniform spherical and surface quite smooth, this implies the silica layer deposited on the surface of $Fe_3O_4$ can reduce the agglomeration process among of particles. In addition, the SEM image of

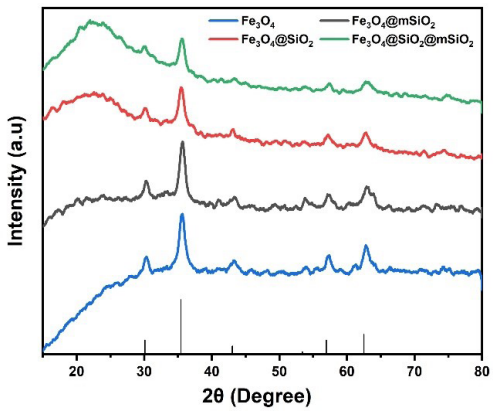


**Figure 2**: XRD patterns of magnetite and composites.

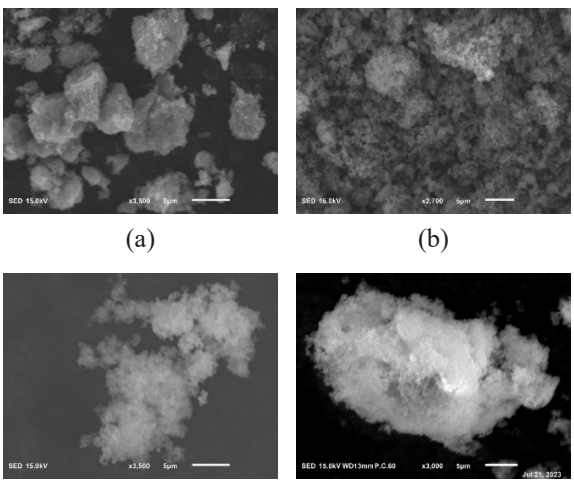


**Figure 3**: SEM images of (a) $Fe_3O_4$, (b) $Fe_3O_4$@$SiO_2$, (c) $Fe_3O_4$@$mSiO_2$, and (d) $Fe_3O_4$@$SiO_2$@$mSiO_2$.

composites $Fe_3O_4$@$mSiO_2$ [Figure 3(c)] and $Fe_3O_4$@$SiO_2$@$mSiO_2$ [Figure 3(d)] showed spherical and uniform morphology. Elemental analysis of magnetite and composites demonstrated the purity and elements. The pure magnetite detected the percentage of Fe and O at 81.45% and 18.55%, respectively. Also, all of the composites were found to be silica with different percentages, for mesoporous and silica shell forms detected at 17.67% and 19.84%. Meanwhile, the combination shell and mesoporous showed the highest content of silica at 31.35% (Table S3). It was confirmed that the morphology of silica affects the amount of silica

The Bruneur-Emmet-Teller (BET) and Barrett-

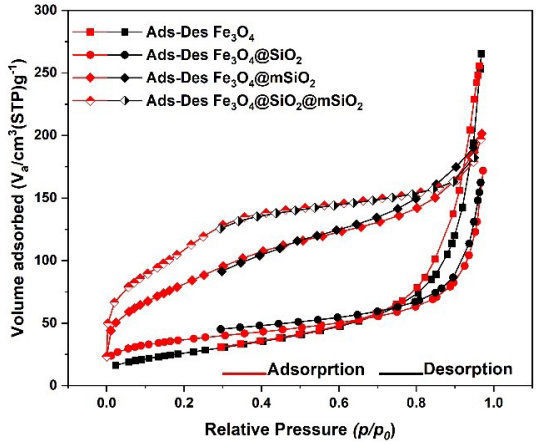


**Figure 4**: $N_2$ adsorption-desorption of $Fe_3O_4$ and their composite.

Joyner-Halenda (BJH) model confirmed the specific surface area and pore size of pure iron oxide, and their composite was characterized by $N_2$ adsorption-desorption. Figure 4 displayed the nitrogen adsorption-desorption isotherm of magnetite and their composite. Bare $Fe_3O_4$ and $Fe_3O_4$@$SiO_2$ are classified as IUPAC type II curves, which suggest the bare $Fe_3O_4$ and $Fe_3O_4$@$SiO_2$ have nonporous and microporous structures [34]. Whereas, $Fe_3O_4$@$mSiO_2$ and $Fe_3O_4$@$SiO_2$@$mSiO_2$ can be classified as a Type IV pattern associated with the existence of mesoporous structure [22]. The BET-specific surface area of $Fe_3O_4$ was 97.02 $m^2.g^{-1}$ after modification $Fe_3O_4$@$SiO_2$, $Fe_3O_4$@$mSiO_2$, and $Fe_3O_4$@$SiO_2$@$mSiO_2$ surface area were significantly increased to 132.80 $m^2.g^{-1}$, 292.74 $m^2.g^{-1}$ and 421.88 $m^2.g^{-1}$, respectively. This means that modification using a different structure of the silica layer on the $Fe_3O_4$ surface can increase the surface area of the magnetite material [22]. The large surface area of $Fe_3O_4$@$SiO_2$@$mSiO_2$ can improve the high load capacity, and the medium porous structure can increase the adsorption capacity of parabens. Therefore, it was chosen because it has good potential as an adsorbent compared to other magnetic adsorbent materials [35]. The pore size distribution of the magnetic and their composites was measured by BJH. After modification with silica, the mean pore diameter of the material decreased, which was related to the increase in the specific surface area of the material (Table S4).

Figure 5 shows the magnetic properties of bare $Fe_3O_4$ and composites performed by VSM analysis.

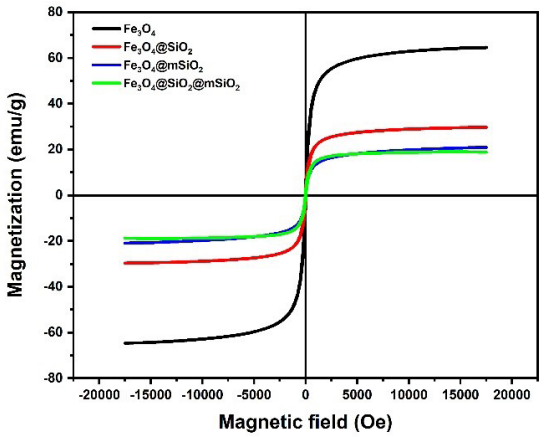


**Figure 5**: Magnetic hysteresis loops of magnetite and the composites.

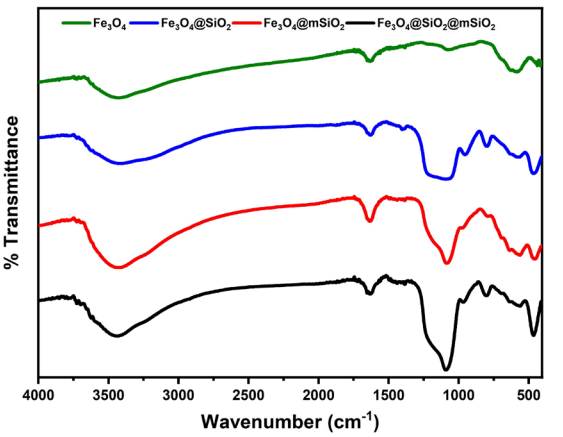


**Figure 6**: FTIR Spectra of magnetite and the composites.

For $Fe_3O_4$ particles, the value of magnetic saturation (Ms) is 64.68 emu/g with no hysteresis loop, which indicates magnetite particles have superparamagnetic properties [36]. The present silica layer on the surface magnetite can reduce magnetic saturation value, all of the composites $Fe_3O_4$@$SiO_2$, $Fe_3O_4$@m$SiO_2$, and $Fe_3O_4$@$SiO_2$@m$SiO_2$ still have superparamagnetic properties with saturation magnetization of 29.67, 20.96 and 18.96 emu/g, respectively. The magnetic saturation value decreases because of the layer diamagnetic properties of silica. In addition, the morphology of the silica layer can affect the magnetization value. Mesoporous silica has a lower magnetization value than shell due to the presentation of Fe in shell structure more than in mesoporous structure (EDX data).

FTIR spectra of bare $Fe_3O_4$ and composites were obtained using the KBR pellet method and recorded from 4000 to 400 $cm^{-1}$. Figure 6 shows the spectra of bare $Fe_3O_4$ particles synthesized by co-precipitation. The vibrational peak at 578 $cm^{-1}$ is related to the Fe-O bond [37], and broad peaks at 1628 and 3400 $cm^{-1}$ are correlated with stretching vibration O-H from water molecule that exists in the iron lattice [38]. The spectrum of magnetite-coated silica has new peaks detected. Vibration bands at 463, 797 and 1096 $cm^{-1}$ are correlated to the vibration band Si-O [38], Si-O-Fe [29], and Si-O-Si vibration [39] respectively. FTIR results suggest the successful coating of the silica layer on the surface of $Fe_3O_4$ particles.

The intermolecular interaction in hydrophobic deep eutectic solvent and ferrofluid was identified by FTIR analysis. Figure 7(a) shows FTIR spectra for menthol as a hydrogen bond acceptor exhibits the vibrational band to the hydroxyl group at 3359 $cm^{-1}$, while the fatty acid as a hydrogen bond donor representative carboxylic group band at 1711 $cm^{-1}$ in the FTIR spectrum.

Figure 7(b) shows FTIR spectra for hydrophobic deep eutectic solvent. The formation HDES can be evaluated through intermolecular interaction via hydrogen bonding between menthol and fatty acid, the pure menthol FTIR Spectrum shows the O-H stretching vibration shifting from 3359 $cm^{-1}$ [Figure 7(a)] to 3379 $cm^{-1}$ in the HDES form [Figure 7(b)]. The shifting O-H vibration indicates the formation of a hydrogen bond between the menthol and the fatty acid, with the electron cloud of the oxygen (O) atom moving towards the hydrogen bond, increasing the force constant, thus causing a blue shift of O-H [40].

Then, the interaction between HDES and $Fe_3O_4$@$SiO_2$@m$SiO_2$ in ferrofluid can be seen from the following shifting wavenumbers in HDES [Figure 7(b)], and ferrofluid [Figure 7(c)]. There was shifting vibration of the O-H band after the formation of $Fe_3O_4$@$SiO_2$@m$SiO_2$-HDES ferrofluid at 3434 $cm^{-1}$ as compared to the O-H band in HDES (3379 $cm^{-1}$). This phenomenon may occur because the surface of the $Fe_3O_4$@$SiO_2$@m$SiO_2$-HDES adsorbent is covered by HDES, which acts as a hydroxyl-functionalized agent [41].

Figure 8 shows the thermogravimetric analysis of composite $Fe_3O_4$@$SiO_2$@m$SiO_2$ and ferrofluid. The thermal stability was carried out over a temperature

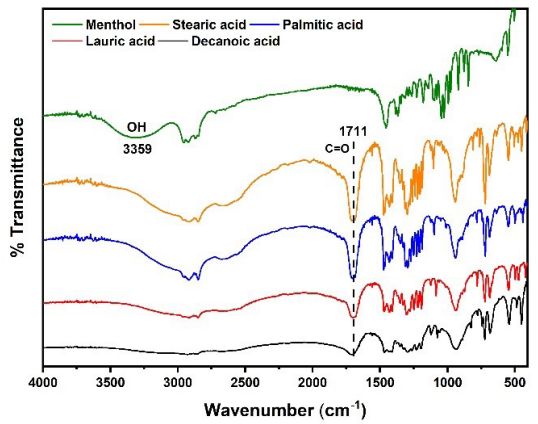


(a)

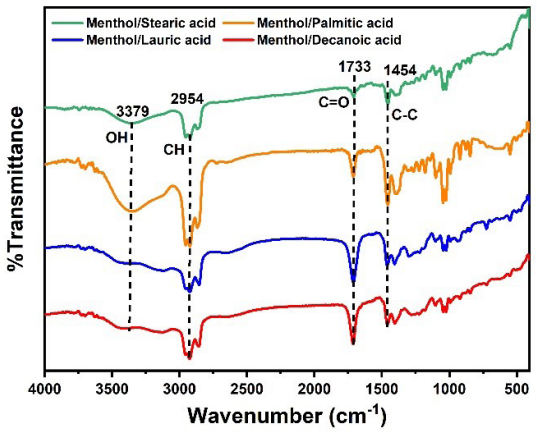


(b)

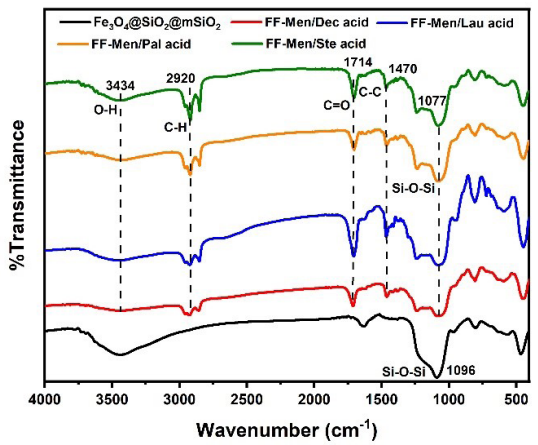


(c)

**Figure 7**: FTIR spectra of (a) menthol and fatty acid, (b) HDES, and (c) Ferrofluids.

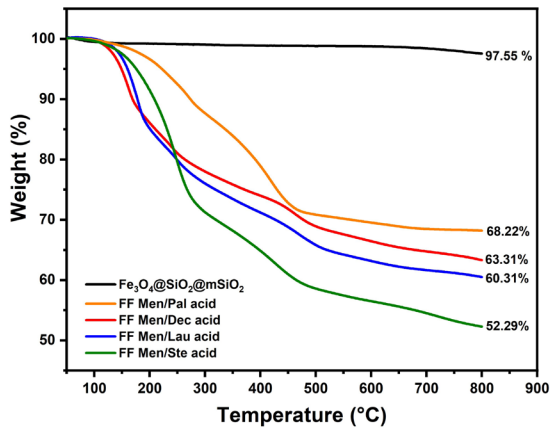


**Figure 8**: Thermogravimetric spectra from ferrofluids.

range from 50–800 ºC with a heating rate of 20 ºC $min^{-1}$. For magnetic composite $Fe_3O_4$@$SiO_2$@m$SiO_2$, it shows an insignificant weight loss of about 2.44%, which was caused by residual water trapped on the surface material. In addition, for all of the ferrofluid below 200 ºC, the percentage weight loss is quite small because of residual from water. After the temperature was raised to 500 ºC, the weight loss was significantly decreased because menthol and fatty acid were decomposed [40]. Temperature from 500–800 ºC shows the weight loss was not significant, which indicated only $Fe_3O_4$@$SiO_2$@m$SiO_2$ was present.

### 3.3 *Sorption performance*

#### *3.3.1 Effect of magnetic types, weight, and carrier liquid*

Ferrofluid is synthesized based on a combination of magnetic particles dispersed in the carrier liquid. Different types of magnetic particles were prepared in the form of $Fe_3O_4$, $Fe_3O_4$@$SiO_2$, $Fe_3O_4$@m$SiO_2$, and $Fe_3O_4$@$SiO_2$@m$SiO_2$. On the other hand, ferrofluids were also prepared by different carrier liquids (water and menthol/decanoic acid). Figure 9(a) shows the percentage of removal of propylparaben with different types of magnetics and carrier liquid treatment. The surface area of the magnetic material has a key role in the adsorption activity, with the percentage of removal propylparaben increasing in line with the surface area of the magnetic materials [Table S2(a)]. This result is consistent with BET analysis showing that, among the

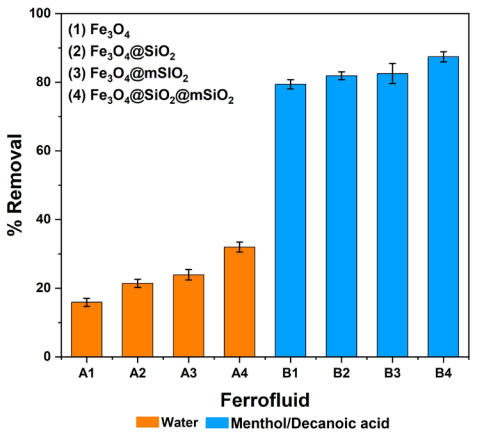


(a)

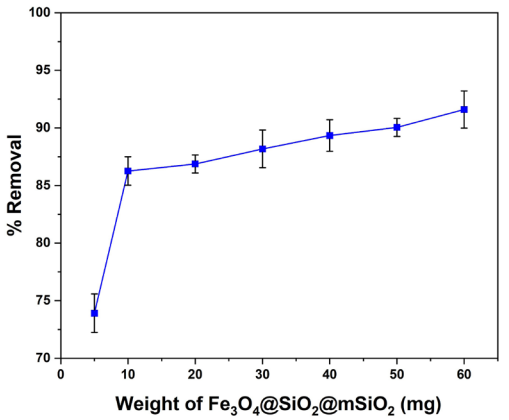


(b)

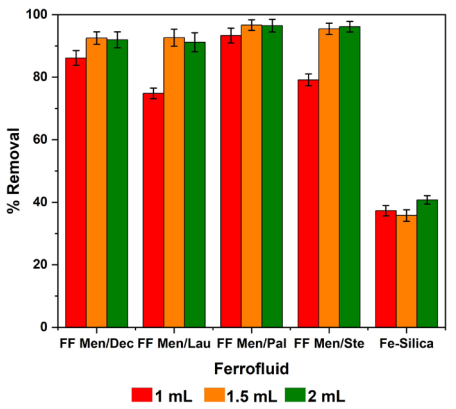


(c)

**Figure 9**: Optimization of propylparaben removal using ferrofluid under various parameters including (a) magnetics and carrier liquids, (b) weight of magnetic, and (c) volume of HDES.

four magnetic particles used, $Fe_3O_4$@$SiO_2$@m$SiO_2$ has a better surface area than other magnetic materials. The large porous surface area of $Fe_3O_4$@$SiO_2$@m$SiO_2$ became one of the ways to adsorb propylparaben (Figure 10). In addition, the carrier liquid also influences the adsorption of propylparaben. The ferrofluid formed by using magnetic material in HDES as the carrier fluid has better performance in removing propylparaben than water as the carrier fluid. The hydrophobicity interaction between propylparaben and HDES can accelerate the absorption process [Figure 9(a)]. Based on the initial performance results of ferrofluid tests in the removal of propylparaben, ferrofluid combination between $Fe_3O_4$@$SiO_2$@m$SiO_2$ and HDES (menthol/decanoic acid) was selected for further studies.

The weight of magnetic in the ferrofluid is also a crucial parameter, Appropriate amounts of magnetic material in the ferrofluid system are one way to improve the ferrofluid's ability to adsorb propylparaben. Figure 9(b) shows the impact of weight $Fe_3O_4$@$SiO_2$@m$SiO_2$ in the ferrofluid system on the adsorption activity of propylparaben. Percent removal of propylparaben increased in line with weight $Fe_3O_4$@$SiO_2$@m$SiO_2$, however at the condition of 60 mg particles in 1 mL of HDES after 1 h stirring at room temperature, it is unstable [Table S2(b)]. Some parts of $Fe_3O_4$@$SiO_2$@m$SiO_2$ were slowly released in the aqueous system, resulting in weakening the ability of HDES to hold $Fe_3O_4$@$SiO_2$@m$SiO_2$ to remain in the ferrofluid system due to the large number of $Fe_3O_4$@$SiO_2$@m$SiO_2$ particles [42]. Therefore, the 50 mg of $Fe_3O_4$@$SiO_2$@m$SiO_2$ was chosen for further study.

Optimization of the paraben removal was also studied using different volumes of HDES. Three different volumes of HDES were prepared with different HDES, and the performance of ferrofluids was studied based on the effectivity in the removal of propylparaben. Figure 9(c) shows the effect of different types of HDES and volume ratio. Based on the data obtained, in general, ferrofluid with a combination of 50 mg in 1.5 mL HDES showed the highest percent removal compared to 1 mL and 2 mL [Table S2(c)]. The increase in the percent removal from ratio A to ratio B is due to an increase in accessible sites, but in ratio C, the percent removal was decreased because of the attributed HDES agglomeration of $Fe_3O_4$@$SiO_2$@m$SiO_2$ in the ferrofluid system [41].

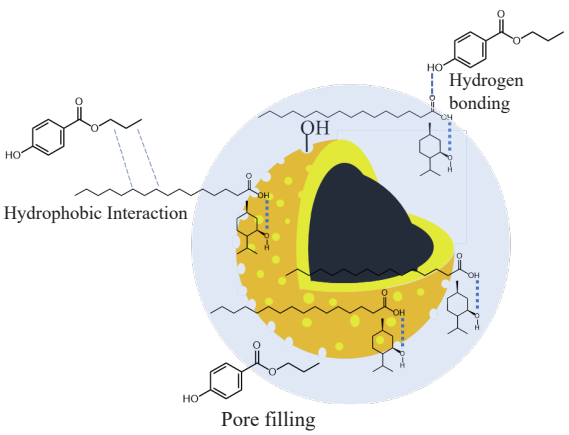


**Figure 10**: Proposed interaction between propylparaben and ferrofluid ($Fe_3O_4$@$SiO_2$@$mSiO_2$ -HDES).

*3.3.2 Effect of ferrofluid volume*

The amount of adsorbent becomes one of the important parameters in the adsorption study. The volume of adsorbent was assessed from 50–250 µL and kept the sample volume constant [41]. Based on the data obtained in Figure 11(a) trend of adsorption removal is increased in line with ferrofluid volume used from 50–200 µL. The increasing amount of ferrofluid would contribute to more active site interaction between ferrofluid and analyte. However, when the volume of ferrofluid was increased up to 250 µL the percent removal was constant (Table S5). This observation indicates that the process of adsorption has reached equilibrium [43].

*3.3.3 Effect of pH of samples*

One of the significant factors affecting the adsorption performance is sample solution pH. The pH of the sample solution was studied from 3.0 to 9.0 on the behavior of propylparaben adsorption. Propylparaben is a compound that is stable at pH 5–6.5, and it can be hydrolyzed in acidic conditions. In addition, they could be negatively charged at pH > 6.5. Figure 11(b) shows that from pH 3–5, the percent removal slowly increases and is stable at pH 6, after that from, pH 7 to 9, the trend gradually decreases (Table S6). The electrostatic repulsion between ferrofluid and propylparaben is due to the deprotonation of the propylparaben molecules [43].

*3.3.4 Effect of adsorption time*

Optimization of time for removal was carried out in the range of 15–90 min. Figure 11(c) shows the result for the percentage removal of propylparaben. Overall, the result revealed that the percentage removal of propylparaben increased from 15 to 30 min, and after that, it tended to decrease and remain constant (Table S7). It could be assumed that the adsorption process occurs quickly, with the availability of active site ferrofluid and easily accessible contact molecule propylparaben. After that, all of the active sites of ferrofluid are saturated with propylparaben, so the adsorption and desorption process begins. Thus, the optimal time and balance system were obtained at 15 min [44].

*3.3.5 Effect of ionic strength of samples*

The addition of salt in the analyte solution to test adsorption performance by changing the ionic strength of the analyte solution is known as the salting-out effect in the range of 1–20% (w/v) NaCl concentration. Figure 11d shows that by increasing NaCl concentration, the percentage adsorption of propylparaben does not change dramatically with a percentage enhanced slightly. Increasing adsorption occurs in the range of NaCl 1–10% (Table S8). It is due to the presence of salt that can reduce the solubility of the analyte and increase ionic strength so that the solution is easy to adsorb on the ferrofluid. Then, the decrease in efficiency of adsorption from 10–20% is due to the decrease in the diffusion rate of the analyte from the enhanced viscosity of the analyte [45].

From the above parameters, a combination of ferrofluid menthol/palmitic acid as a carrier of magnetic material has the highest efficiency when compared to others. Meanwhile, $Fe_3O_4$@$SiO_2$@$mSiO_2$ has the lowest percentage removal ability, even though $Fe_3O_4$@$SiO_2$@$mSiO_2$ has a large surface area.

In general, increasing the carbonyl chain in fatty acid (hydrogen bond donor) in the ferrofluid increases the adsorption percentage of propylparaben. This can be attributed to several factors, such as increasing the viscosity of the solution causing a decrease in mass transfer efficiency, then increasing the carbon chain might facilitate the substance [31]. In addition, factors such as hydrophobicity and stability in water are

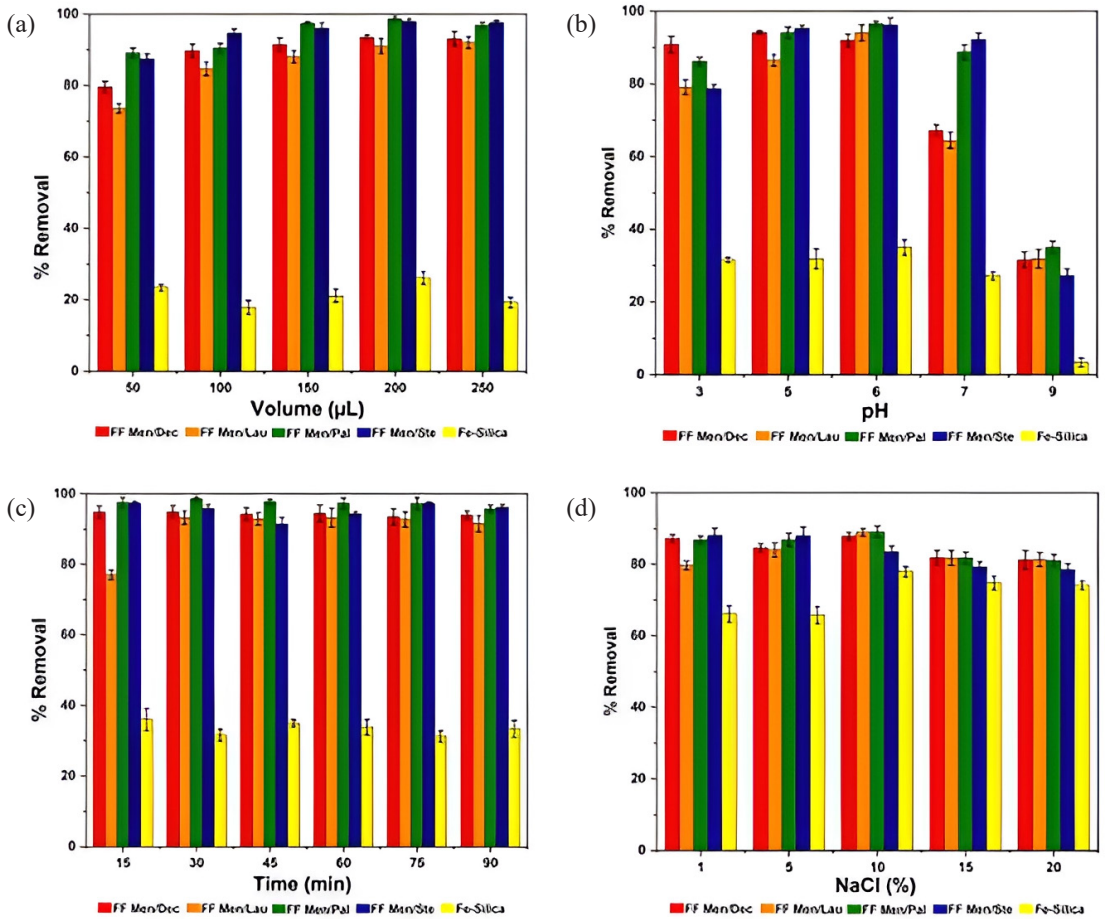


**Figure 11**: Parameters in ferrofluid adsorption (a) volume, (b) pH, (c) time, and (d) Ionic strength.

generally influenced by the alkyl chain of individual components that affect the efficiency percentage [46]. Meanwhile, the decrease in extraction in the combination of menthol/stearic acid is due to the instability of components at lower 30 ºC, hydrophobic DES does not last long and forms a white crystalline phase, which causes efficiency to decrease [47].

### *3.3.6 Investigation of performance of ferrofluid in paraben series*

Methylparaben (MP), ethylparaben (EP), Propylparaben (PP), and butylparaben (BP) were chosen as paraben series and evaluated the performance of ferrofluid menthol/palmitic acid. Figure 12 shows the performance of ferrofluid menthol/palmitic in different paraben solutions, the data percent removal displays that

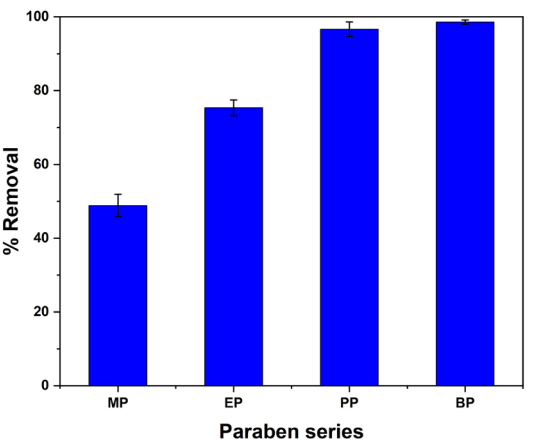


**Figure 12**: Ferrofluid menthol/palmitic acid performance in paraben series.

butylparaben has a higher percent removal than others (Table S9). Commonly, the solubility of paraben in water would reduce as their alkyl chain length, which follows methyl< ethyl< propyl< butyl [48], and the data from log KOW show that butylparaben has higher hydrophobicity than others. So, the interaction between HBD ferrofluid and paraben is influenced by hydrophobicity from carbon chain length [49].

## 4 Conclusions

An efficient, simple, and green sorbent-based $Fe_3O_4$@$SiO_2$@m$SiO_2$-HDES has been as adsorption for parabens purposes. The ferrofluid, composed of $Fe_3O_4$@$SiO_2$@m$SiO_2$-menthol/palmitic acid, has prominent advantages over the other magnetic ferrofluids. The higher presentation removal of paraben achieved values ranging from 81.00–98.62% by $Fe_3O_4$@$SiO_2$@m$SiO_2$-menthol/palmitic. The $Fe_3O_4$@$SiO_2$@m$SiO_2$-HDES ferrofluid technique was offered simple, environmentally friendly, consumed low volume of sorbent, and room temperature process was achieved. Ferrofluid $Fe_3O_4$@$SiO_2$@m$SiO_2$-HDES also improves the separation process by eliminating the centrifugated with an external magnet.

## Acknowledgments

This research is funded by the Thailand Science Research and Innovation Fund Chulalongkorn University (DIS66230004). The authors gratefully acknowledge the financial support by ASEAN-NON ASEAN Scholarship-Chulalongkorn University.

## Author Contributions

A.F.: investigation, methodology, data analysis, writing an original draft; N.I.: investigation, reviewing, and editing. All Authors have read and agreed to the published version of the manuscript.

## Conflict of Interest

The authors declare no conflict of interest.

## References

[1] M. de los Á. B. del H. Bueno, N. Boluda-Botella, and D. P. Rico, "Removal of emerging pollutants in water treatment plants: Adsorption of methyl and propylparaben onto powdered activated carbon," *Adsorption*, vol. 25, no. 5, pp. 983–999, 2019, doi: 10.1007/s10450-019-00120-7.

[2] P. Gupta and K. Pushkala, "Parabens: The love-hate molecule," *Clinical Journal of Obstetrics and Gynecology*, vol. 3, no. 1, pp. 037–038, 2020, doi: 10.29328/journal.cjog.1001047.

[3] Z. Petric, J. Ruzic, and I. Zuntar, "The controversies of parabens–An overview nowadays," *Acta Pharmaceutica*, vol. 71, pp. 17–32, 2021, doi: 10.2478/acph-2021-0001.

[4] K. Nowaka, W. Ratajczak–Wronaa, M. Górskab, and E. Jabłońskaa, "Parabens and their effects on the endocrine system," *Molecular and Cellular Endocrinology*, vol. 474, pp. 238–251, 2018, doi: 10.1016/j.mce.2018.03.014.

[5] J. Kapelewska, U. Kotowska, J. Karpińska, D. Kowalczuk, A. Arciszewska, and A. Świrydo, "Occurrence, removal, mass loading, and environmental risk assessment of emerging organic contaminants in leachates, groundwaters, and wastewaters," *Microchemical Journal*, vol. 137, pp. 292–301, 2018, doi: 10.1016/j.microc.2017.11.008.

[6] E. Carmona, V. Andreu, and Y. Picó, "Occurrence of acidic pharmaceuticals and personal care products in Turia River Basin: From waste to drinking water," *Science of the Total Environment*, vol. 484, pp. 53–63, 2014, doi: 10.1016/j.scitotenv.2014.02.085.

[7] A. M. C. Ferreira, M. Möder, and M. E. F. Laespada, "GC-MS determination of parabens, triclosan and methyl triclosan in water by in situ derivatisation and stir-bar sorptive extraction," *Analytical and Bioanalytical Chemistry*, vol. 399, pp. 945–953, 2011, doi: 10.1007/s00216-010-4339-7.

[8] X. Zhaoa, W. Qiu, Y. Zheng, J. Xiong, C. Gao, and S. Hu, "Occurrence, distribution, bioaccumulation, and ecological risk of bisphenol analogues, parabens, and their metabolites in the Pearl River Estuary, South China," *Ecotoxicology and Environmental Safety*, vol. 180, pp. 43–52, 2019, doi: 10.1016/j.ecoenv.2019.04.083.

[9] G. Guo, Y. Wang, T. Hao, D. Wu, and G. H. Chen, "Enzymatic nitrous oxide emissions from

wastewater treatment," *Frontries of Environmental Science and Engineering*, vol. 12, no. 1, pp. 1–12, 2018, doi: 10.1007/s11783-018-1021-3.

[10] A. A. Basfar and F. A. Rehim, "Disinfection of wastewater from a Riyadh wastewater treatment plant with ionizing radiation," *Radiation Physics and Chemistry*, vol. 65, no. 4–5, pp. 527–532, 2002, doi: 10.1016/S0969-806X(02)00346-8.

[11] J. H. Luo, J. Li, Y. B. Qi, and Y. Q. Cao, "Study on the removal of chromium(III) by solvent extraction," *Desalination and Water Treatment*, vol. 51, no. 10–12, pp. 2130–2134, 2013, doi: 10.1080/19443994.2012.735404.

[12] F. Chen, M. Lv, Y. Ye, S. Miao, X. Tang, Y. Liu, B. Liang, Z. Qin, Y. Chen, Z. He, and Y. Wang, "Insights on uranium removal by ion exchange columns: The deactivation mechanisms, and an overlooked biological pathway," *Chemical Engineering Journal*, vol. 434, 2022, Art. no. 134708, doi: 10.1016/j.cej.2022.134708.

[13] A. Pohl, "Removal of heavy metal ions from water and wastewaters by sulfur-containing precipitation agents," *Water, Air, and Soil Pollution*, vol. 231, no. 10, pp. 1–17, 2020, doi: 10.1007/s11270-020-04863-w.

[14] M. Darvishmotevallia, A. Zarei, M. Moradnia, M. Noorisepehr, and H. Mohammadi, "Optimization of saline wastewater treatment using electrochemical oxidation process: Prediction by RSM method," *MethodsX*, vol. 6, pp. 1101–1113, 2019, doi: 10.1016/j.mex.2019.03.015.

[15] Z. Sun, D. Huang, X. Duan, W. Honga, and J. Lianga, "Functionalized nanoflower-like hydroxyl magnesium silicate for effective adsorption of aflatoxin B1," *Journal of Hazardous Materials*, vol. 387, 2020, doi: 10.1016/j.jhazmat.2019.121792.

[16] X. Zhao, L. Liu, N. Li, T. Wang, Y. Chai, Z. Yang, J. Ye, Q. Chu, and L. Chen, "Zeolite silica nanoparticles-supported open-tubular columns for isomer and chiral separation using capillary electrochromatography coupled with amperometric detection," *New Journal of Chemistry*, vol. 44, no. 3, pp. 1028–1035, 2020, doi: 10.1039/c9nj04859f.

[17] P. González-Hernández, A. Gutiérrez-Serpa, A. B. Lago, L. Estévez, J. H. Ayala, V. Pino, and J. Pasán, "Insights into paraben adsorption by metal-organic frameworks for analytical applications," *ACS Applied Materials and Interfaces*, vol. 13, no. 38, pp. 45639–45650, 2021, doi: 10.1021/acsami.1c14416.

[18] A. Duque, J. Grau, J. L. Benede, R. M. Alonso, M. A. Campanero, and A. Chisvert, "Low toxicity deep eutectic solvent-based ferrofluid for the determination of UV filters in environmental waters by stir bar dispersive liquid microextraction," *Talanta*, vol. 243, pp. 1–10, 2022, doi: 10.1016/j.talanta.2022.123378.

[19] L. Shen, Y. Qiao, Y. Guo, S. Meng, G. Yang, M. Wu, and J. Zhao, "Facile co-precipitation synthesis of shape-controlled magnetite nanoparticles," *Ceramics International*, vol. 40, no. 1, pp. 1519–1524, 2014, doi: 10.1016/j.ceramint.2013.07.037.

[20] J. F. Liu, Z. S. Zhao, and G. B. Jiang, "Coating $Fe_3O_4$ magnetic nanoparticles with humic acid for high efficient removal of heavy metals in water," *Environmental Science and Technology*, vol. 42, no. 18, pp. 6949–6954, 2008, doi: 10.1021/es800924c.

[21] K. Xu, Y. Wang, Y. Li, Y. Lin, H. Zhang, and Y. Zhou, "A novel poly(deep eutectic solvent)-based magnetic silica composite for solid-phase extraction of trypsin," *Analytica Chimica Acta*, vol. 946, pp. 64–72, 2016, doi: 10.1016/j.aca.2016.10.021.

[22] H. Lu, and S. Xu, "Mesoporous structured estrone imprinted $Fe_3O_4$@$SiO_2$@m$SiO_2$ for highly sensitive and selective detection of estrogens from water samples by HPLC," *Talanta*, vol. 144, pp. 303–311, 2015, doi: 10.1016/j.talanta.2015.06.017.

[23] F. Mehrabi, M. Ghaedi, and E. A. Dil, "Magnetic nanofluid based on hydrophobic deep eutectic solvent for efficient and rapid enrichment and subsequent determination of cinnamic acid in juice samples: Vortex-assisted liquid-phase microextraction," *Talanta*, vol. 260, 2023, Art. no. 124581, doi: 10.1016/j.talanta.2023.124581.

[24] T. Gu, M. Zhang, J. Chen, and H. Qiu, "A novel green approach for the chemical modification of silica particles based on deep eutectic solvents," *Chemical Communications*, vol. 51, no. 48, pp. 9825–9828, 2015, doi: 10.1039/c5cc02553b.

[25] D. Jose, A. Tawai, D. Divakaran, D. Bhattacharyya, P. Venkatachalam, P. Tantayotai, and M. Sriariyanun, "Integration of deep eutectic solvent in biorefining process of lignocellulosic biomass valorization," *Bioresource Technology Reports*, vol. 21, 2023, Art. no. 101365, doi: 10.1016/j.biteb.2023.101365.

[26] C. Florindo, L. C. Branco, and I. M. Marrucho, "Development of hydrophobic deep eutectic solvents for extraction of pesticides from aqueous environments," *Fluid Phase Equilibria*, vol. 448, pp. 135–142, 2017.

[27] E. A. Dil, M. Ghaedi, A. Asfaram, L. Tayebi, and F. Mehrabi, "A ferrofluidic hydrophobic deep eutectic solvent for the extraction of doxycycline from urine, blood plasma and milk samples prior to its determination by high-performance liquid chromatography-ultraviolet," *Journal of Chromatograohy A*, vol. 1613, 2020, Art. no. 460695, doi: 10.1016/j.chroma.2019.460695.

[28] Ö. Demir, "Synthesis of $Fe_3O_4$ magnetic nanoparticles, and investigation of removal capacity," *Journal of the Chemical Society Pakistan*, vol. 40, no. 01, pp. 111–122, 2018, doi: 10.21175/rad.abstr.book.2021.15.5.

[29] S. Pirsa and F. Asadzadeh, "Synthesis of $Fe_3O_4$/$SiO_2$/Polypyrrole magnetic nanocomposite polymer powder: Investigation of structural properties, and ability to purify of edible sea salts," *Advanced Powder Technology*, vol. 32, no. 4, pp. 1233–1246, 2021, doi: 10.1016/j.apt.2021.02.027.

[30] H. Tabasi, M. T. H. Mosavian, M. Darroudi, M. Khazaei, A. Hashemzadeh, and Z. Sabouri, "Synthesis and characterization of amine-functionalized $Fe_3O_4$/mesoporous silica nanoparticles (MSNs) as potential nanocarriers in drug delivery systems," *Journal of Porous Materials*, vol. 29, no. 6, pp. 1817–1828, 2022, doi: 10.1007/s10934-022-01259-5.

[31] T. Kriížek, M. Bursová, R. Horsley, M. Kuchař, P. Tůma, R. Čabala, T. Hložek, "Menthol-based hydrophobic deep eutectic solvents: Towards greener and efficient extraction of phytocannabinoids," *Journal of Cleaner Production*, vol. 193, pp. 391–396, 2018.

[32] W. M. Daoush, "Co-Precipitation and magnetic properties of magnetite nanoparticles for potential biomedical applications," *Journal of Nanomedicine Research*, vol. 5, no. 1–6, 2017, doi: 10.15406/jnmr.2017.05.00118.

[33] G. Antarnusa, P. D. Jayanti, Y. R. Denny, and A. Suherman, "Utilization of co-precipitation method on synthesis of $Fe_3O_4$/PEG with different concentrations of PEG for biosensor applications," *Materialia*, vol. 25, 2022, Art. no. 101525, doi: 10.1016/j.mtla.2022.101525.

[34] J. Ma, N. Sun, C. Wang, J. Xue, and L. Qiang, "Facile synthesis of novel $Fe_3O_4$@$SiO_2$@$mSiO_2$@$TiO_2$ core-shell microspheres with mesoporous structure and their photocatalytic performance," *Journal of Alloys and Compounds*, vol. 743, pp. 456–463, 2018, doi: 10.1016/j.jallcom.2018.02.005.

[35] Y. Zhang, F. Jiang, D. Huang, S. Hou, H. Wang, M. Wang, Y. Chi, and Z. Zhao, "A facile route to magnetic mesoporous core-shell structured silicas containing covalently bound cyclodextrins for the removal of the antibiotic doxycycline from water," *RSC Advances*, vol. 8, no. 55, pp. 31348–31357, 2018, doi: 10.1039/c8ra05781h.

[36] H. E. Ghandoor, H. M. Zidan, M. M. H. Khalil, and M. I. M. Ismail, "Synthesis and some physical properties of magnetite ($Fe_3O_4$) nanoparticles," *International Journal of Electrochemical Science*, vol. 7, pp. 5734–5745, 2012, doi: 10.1016/S1452-3981(23)19655-6.

[37] C. A. Dincer, N. Yıldız, N. Aydogan, and A. Calımlı, "A comparative study of $Fe_3O_4$ nanoparticles modified with different silane compounds," *Applied Surface Science*, vol. 318, pp. 297–304, 2014, doi: 10.1016/j.apsusc.2014.06.069.

[38] C. Ma, C. Li, N. He, F. Wang, N. Ma, L. Zhang, Z. Lu, Z. Ali, Z. Xi, X. Li, G. Liang, H. Liu, Y. Deng, L. Xu, and Z. Wang, "Preparation and characterization of monodisperse Core–Shell $Fe_3O_4$@$SiO_2$ microspheres and its application for magnetic separation of nucleic acids from *E. coli* BL21," *Journal of Biomedical Nanotecnology*, vol. 8, pp. 1000–1005, 2012, doi: 10.1166/jbn.2012.1454.

[39] M. A. Mustafa, Q. A. Qasim, A. B. Mahdi, S. E. Izzar, Y. S. Alnassar, E. S. Abood, Z. J. Alhakim, Z. H. Mahmoud, A. M. Rheima, and H. N. K. Al-Salman, "Supercapacitor

performance of $Fe_3O_4$, and $Fe_3O_4$@$SiO_2$-bis(aminopyridine)-Cu hybrid nanocomposite," *International Journal of Electrochemical Science*, vol. 17, no. 10, 2022, Art. no. 221057, doi: 10.20964/2022.10.49.

[40] Z. Lin, Y. Zhang, Q. Zhao, A. Chen, and B. Jiao, "Ultrasound-assisted dispersive liquid-phase microextraction by solidifying L-menthol-decanoic acid hydrophobic deep eutectic solvents for detection of five fungicides in fruit juices and tea drinks," *Journal of Separation Science*, vol. 44, no. 20, pp. 3870–3882, 2021, doi: 10.1002/jssc.202100590.

[41] R.E.A. Mohammad, A.A. Elbashir, J. Karim, N. Yahaya, N. Y. Rahim, and M. Miskam, "Development of deep eutectic solvents based ferrofluid for liquid phase microextraction of ofloxacin, and sparfloxacin in water samples," *Microchemical Journal*, vol. 181, 2022, Art. no. 107806, doi: 10.1016/j.microc.2022.107806.

[42] H. Piao, Y. Jiang, Z. Qin, P. Ma, Y. Sun, X. Wang, D. Song, and Q. Fei, "Application of an in-situ formulated magnetic deep eutectic solvent for the determination of triazine herbicides in rice," *Talanta*, vol. 222, 2021, Art. no. 121527, doi: 10.1016/j.talanta.2020.121527.

[43] H. R. Nodeha, H. Sereshtib, S. Ataolahib, A. Toloutehrani, and A. T. Ramezanib, "Activated carbon derived from pistachio hull biomass for the effective removal of parabens from aqueous solutions: isotherms, kinetics, and free energy studies," *Desalination and Water Treatment*, vol. 201, pp. 155–164, 2020, doi: 10.5004/dwt.2020.25985.

[44] D. Yanga, G. Li, L. Wu, and Y. Yanga, "Ferrofluid-based liquid-phase microextraction: Analysis of four phenolic compounds in milks and fruit juices," *Food Chemistry*, vol. 261, pp. 96–102, 2018, doi: 10.1016/j.foodchem.2018.04.038.

[45] N. Nouri and H. Sereshti, "Electrospun polymer composite nanofiber-based in-syringe solid phase extraction in tandem with dispersive liquid-liquid microextraction coupled with HPLC-FD for determination of aflatoxins in soybean," *Food Chemistry*, vol. 289, pp. 33–39, 2019, doi: 10.1016/j.foodchem.2019.03.026.

[46] A. R. Zarei, M. Nedaei, and S. A. Ghorbanian, "Ferrofluid of magnetic clay and menthol based deep eutectic solvent: Application in directly suspended droplet microextraction for enrichment of some emerging contaminant explosives in water and soil samples," *Journal of Chromatography A*, vol. 1553, pp. 32–42, 2018, doi: 10.1016/j.chroma.2018.04.023.

[47] J. M. Silva, C. V. Pereira, F. Mano, E. Silva, V. I. B. Castro, I. Sá-Nogueira, R. L. Reis, A. Paiva, A. A. Matias, and A. R. C. Duarte, "Therapeutic role of deep eutectic solvents based on menthol and saturated fatty acids on wound healing," *Applied Bio Materials*, vol. 2, pp. 4346–4355, 2019, doi: 10.1021/acsabm.9b00598.

[48] B. Kapalavavi, J. Ankney, M. Baucom, and Y. Yang, "Solubility of parabens in subcritical water," *Journal of Chemical and Engineering Data*, vol. 59, no. 3, pp. 912–916, 2014, doi: 10.1021/je4010883.

[49] D. W. Zelinski, F. O. Farias, G. Oliveira, L. Igarashi-Mafra, and M. R. Mafra, "COSMO-SAC model and vortex assisted liquid-liquid microextraction to assess the hydrophobic deep eutectic solvents as an alternative path for parabens removal from aqueous media," *Fluid Phase Equilibria*, vol. 560, 2022, Art. no. 113503, doi: 10.1016/j.fluid.2022.113503.

## Supporting Information

**Table S1**: Variations of ratio synthesis of ferrofluid

| HDES | Menthol (mol) | Fatty acid (mol) |
|---|---|---|
| HDES 1 | Menthol (1) | Decanoid acid (1) |
| HDES 2 | Menthol (1) | Lauric acid (1) |
| HDES 3 | Menthol (12) | Palmitic acid (1) |
| HDES 4 | Menthol (9) | Stearic acid (1) |

**Table S2**: (a) Variations of the ratio between different magnetic types and carrier liquids in the synthesis of ferrofluid

| Material* | % Removal | |
|---|---|---|
| | $H_2O$ | Menthol/ Decanoic Acid |
| $Fe_3O_4$ | 15.88 | 79.40 |
| $Fe_3O_4$@$SiO_2$ | 21.38 | 81.88 |
| $Fe_3O_4$@m$SiO_2$ | 23.91 | 82.54 |
| $Fe_3O_4$@$SiO_2$@m$SiO_2$ | 31.97 | 88.18 |
| *30 mg in 1 mL carrier liquid | | |

**Table S2**: (b) Variations of the ratio between the different weights of magnetic ($Fe_3O_4$@$SiO_2$@m$SiO_2$) and HDES in the synthesis of ferrofluid

| $Fe_3O_4$@$SiO_2$@m$SiO_2$ (mg)* | % Removal |
|---|---|
| 5 | 73.90 |
| 10 | 86.26 |
| 20 | 86.87 |
| 30 | 88.18 |
| 40 | 89.34 |
| 50 | 90.05 |
| 60 | 91.60 |

*in 1 mL menthol/Decanoic acid

**Table S2**: (c) %Removal of ferrofluids with different HDES and magnetic particle: HDES ratio

| Ratio | Ferrofluids | | | | |
|---|---|---|---|---|---|
| | FF Men/Dec | FF Men/Lau | FF Men/Pal | FF Men/Ste | FF Fe-$SiO_2$ |
| Ratio A (50 mg/1 mL) | 86.14 | 74.82 | 93.33 | 79.14 | 37.29 |
| Ratio B (50 mg/1.5 mL) | 92.51 | 92.63 | 96.66 | 95.46 | 35.78 |
| Ratio C (50 mg/2 mL) | 91.95 | 91.19 | 96.48 | 96.14 | 40.04 |

**Table S3**: EDX data of $Fe_3O_4$ and their composite

| Materials | Mass (%) | | | Atom (%) | | |
|---|---|---|---|---|---|---|
| | Fe | O | Si | Fe | O | Si |
| $Fe_3O_4$ | 81.45 | 18.55 | - | 55.70 | 44.30 | - |
| $Fe_3O_4$@$SiO_2$ | 42.39 | 37.78 | 19.84 | 19.83 | 61.71 | 18.46 |
| $Fe_3O_4$@m$SiO_2$ | 37.52 | 44.84 | 17.67 | 16.38 | 68.29 | 15.33 |
| $Fe_3O_4$@$SiO_2$ @m$SiO_2$ | 20.99 | 47.65 | 31.35 | 8.41 | 66.62 | 24.97 |

**Table S4**: Data of surface area and total pore diameter

| Materials | BET Surface Area [$m^2\ g^{-1}$] | Total Pore Volume [$cm^3\ g^{-1}$] | Mean Pore Diameter [nm] |
|---|---|---|---|
| $Fe_3O_4$ | 97.02 | 0.4103 | 16.918 |
| $Fe_3O_4$@$SiO_2$ | 132.80 | 0.2658 | 8.0053 |
| $Fe_3O_4$@ m$SiO_2$ | 292.74 | 0.3049 | 4.2575 |
| $Fe_3O_4$@ $SiO_2$@m$SiO_2$ | 421.88 | 0.3116 | 2.8910 |

**Table S5**: Effect of ferrofluids volumes on %removal of propylparaben

| Volume (µL) | % Removal | | | | |
|---|---|---|---|---|---|
| | FF Men/Dec | FF Men/Lau | FF Men/Pal | FF Men/Ste | FF Fe-$SiO_2$ |
| 50 | 79.57 | 73.57 | 89.11 | 87.39 | 23.35 |
| 100 | 89.69 | 84.57 | 90.39 | 94.57 | 17.87 |
| 150 | 91.41 | 88.04 | 97.4 | 95,99 | 21.09 |
| 200 | 93.41 | 91.06 | 98.62 | 97.86 | 26.09 |
| 250 | 93.05 | 91.97 | 96.83 | 97.6 | 19.23 |

**Table S6**: Effect of pH on %removal of propylparaben

| pH | % Removal | | | | |
|---|---|---|---|---|---|
| | FF Men/Dec | FF Men/Lau | FF Men/Pal | FF Men/Ste | FF Fe-$SiO_2$ |
| 3 | 90.8 | 79.06 | 86.11 | 78.62 | 31.56 |
| 5 | 94.1 | 86.41 | 94.02 | 95.22 | 31.86 |
| 6 | 91.95 | 94.02 | 96.48 | 96.14 | 34.96 |
| 7 | 67.14 | 64.39 | 88.69 | 92.14 | 27.23 |
| 9 | 31.56 | 31.86 | 34.96 | 27.23 | 3.41 |

**Table S7**: Effect of time on %removal of propylparaben

| Time (min) | % Removal | | | | |
|---|---|---|---|---|---|
| | FF Men/Dec | FF Men/Lau | FF Men/Pal | FF Men/Ste | FF Fe-$SiO_2$ |
| 15 | 94.78 | 77.09 | 97.58 | 97.37 | 36.03 |
| 30 | 94.85 | 93.21 | 98.57 | 95.85 | 31.62 |
| 45 | 94.18 | 92.89 | 97.75 | 91.40 | 35.00 |
| 60 | 94.40 | 93.19 | 97.30 | 94.90 | 33.89 |
| 75 | 93.49 | 92.68 | 97.26 | 97.27 | 31.27 |
| 90 | 93.96 | 91.51 | 95.76 | 96.12 | 33.42 |

**Table S8**: Effect of ionic strength on %removal of propylparaben

| NaCl (%) | % Removal | | | | |
|---|---|---|---|---|---|
| | FF Men/Dec | FF Men/Lau | FF Men/Pal | FF Men/Ste | FF Fe-$SiO_2$ |
| 1 | 87.23 | 79.65 | 86.87 | 88.08 | 66.16 |
| 5 | 84.53 | 84.03 | 86.84 | 87.94 | 65.82 |
| 10 | 87.87 | 88.97 | 89.05 | 83.48 | 77.99 |
| 15 | 81.82 | 81.75 | 81.71 | 79.21 | 74.78 |
| 20 | 81.21 | 81.28 | 81.00 | 78.52 | 74.18 |

**Table S9**: % Removal of ferrofluids with different parabens

| Analyte | % Removal |
|---|---|
| Methylparaben (MP) | 48.86 |
| Ethylparaben (EP) | 75.35 |
| Propylparaben (PP) | 96.66 |
| Butylparaben (BP) | 98.58 |